



PAPER

Identification and analysis of stable breathing periods in electrical impedance tomography recordings

RECEIVED
30 March 2021REVISED
19 May 2021ACCEPTED FOR PUBLICATION
7 June 2021PUBLISHED
29 June 2021K Haris^{1,2} , B Vogt³, C Strodthoff³, D Pessoa⁴ , G-A Cheimariotis¹, B Rocha⁴ , G Petmezas¹ , N Weiler³, R P Paiva⁴, P de Carvalho⁴, N Maglaveras^{1,5} and I Frerichs³ ¹ Lab of Computing, Medical Informatics and Biomedical Imaging Technologies, Aristotle University, Thessaloniki, Greece² Department of Informatics and Computer Engineering, University of West Attica, Greece³ Department of Anaesthesiology and Intensive Care Medicine, University Medical Centre Schleswig-Holstein, Campus Kiel, Germany⁴ University of Coimbra, Centre for Informatics and Systems of the University of Coimbra, Department of Informatics Engineering, 3030-290 Coimbra, Portugal⁵ Department of Electrical and Computer Engineering, Northwestern University, Evanston, IL, United States of AmericaE-mail: konharis@gmail.com

Keywords: EIT, electrical impedance tomography, stable tidal breathing, wearable sensors

Abstract

Objective. In this paper, an automated stable tidal breathing period (STBP) identification method based on processing electrical impedance tomography (EIT) waveforms is proposed and the possibility of detecting and identifying such periods using EIT waveforms is analyzed. In wearable chest EIT, patients breathe spontaneously, and therefore, their breathing pattern might not be stable. Since most of the EIT feature extraction methods are applied to STBPs, this renders their automatic identification of central importance. *Approach.* The EIT frame sequence is reconstructed from the raw EIT recordings and the raw global impedance waveform (GIW) is computed. Next, the respiratory component of the raw GIW is extracted and processed for the automatic respiratory cycle (breath) extraction and their subsequent grouping into STBPs. *Main results.* We suggest three criteria for the identification of STBPs, namely, the coefficient of variation of (i) breath tidal volume, (ii) breath duration and (iii) end-expiratory impedance. The total number of true STBPs identified by the proposed method was 294 out of 318 identified by the expert corresponding to accuracy over 90%. Specific activities such as speaking, eating and arm elevation are identified as sources of false positives and their discrimination is discussed. *Significance.* Simple and computationally efficient STBP detection and identification is a highly desirable component in the EIT processing pipeline. Our study implies that it is feasible, however, the determination of its limits is necessary in order to consider the implementation of more advanced and computationally demanding approaches such as deep learning and fusion with data from other wearable sensors such as accelerometers and microphones.

1. Introduction

Electrical impedance tomography (EIT) is a non-invasive functional imaging modality that makes continuous chest examinations possible without any radiation exposure in either adults or children (Brown 2003, Pullett *et al* 2010, Frerichs *et al* 2017, Martins *et al* 2019). Compared to other modalities, EIT is highly portable, it can support short and long-term monitoring and its cost is relatively low. Due to its high temporal resolution, EIT is able to detect dynamic changes in the pulmonary air content in the examined chest plane, a necessary precondition for ventilation distribution assessment and regional ventilation heterogeneity detection.

In a clinical setting, EIT has been used mainly in ICUs for mechanically ventilated patients (Kobylianskii *et al* 2016). These patients typically do not move and their ventilator-controlled breathing pattern is stable allowing the use of a number of well-known and established EIT analysis methods. Recently, the development of wearable EIT systems provided the possibility of monitoring regional lung ventilation in other patient groups as well (for instance, in patients with chronic lung diseases), even outside the hospital (Chouvarda *et al* 2015,

Rapin *et al* 2019). These patients breathe spontaneously, and thus, their breathing pattern is not stable. Effects like body movement, speech, cough, sigh, exercise, change/loss in electrode contact impact the recordings and impose great challenges in automated EIT data analysis.

Specifically, in wearable EIT devices, electrodes are integrated into belts or vests in order to minimize user intervention concerning placement issues like electrode spacing and adjustment. In most EIT device configurations 16 or 32 electrodes are used typically placed in one transverse (or slightly oblique) plane. The main factors influencing chest EIT measurements in wearable EIT, and consequently the identification of stable breathing, are:

- *Electrode contact*—Modern electrodes can sense and continuously monitor the electrode-skin contact quality. Therefore, EIT data acquisition periods corresponding to low-quality electrode contact are detected and either rejected or processed with special methods.
- *Missing/faulty electrodes*—EIT images of best quality are achieved when the EIT signal quality is good at all electrodes (Adler 2004, Hartinger *et al* 2009). Modern EIT wearable vests automatically record electrode contact information during acquisition, enabling the detection of time periods of missing or low quality data.
- *Body movement*—Movement of patients during EIT data acquisition causes significant effects on the recorded measurements (Vogt *et al* 2016). EIT measurements recorded during body movement can be identified through accelerometers.
- *Posture*—EIT data acquisition protocols require specific body posture. However, during various pulmonary manoeuvres, but even during quiet tidal breathing, subjects move involuntarily to facilitate and improve their ventilation (Zhao *et al* 2013, Becher *et al* 2015, Frerichs *et al* 2016, Lehmann *et al* 2016, Lasarow *et al* 2021). The forward movement of the torso and the elevation of the arms cause a significant effect on the EIT waveforms registered during otherwise undisturbed tidal breathing (Vogt *et al* 2016).
- *Type of ventilation*—Clinical studies have shown that the type of ventilation affects the EIT findings (Blankman *et al* 2013, Mauri *et al* 2013, Yoshida *et al* 2013) and, therefore, ventilation type should be recorded to ease the data interpretation. The factors affecting EIT acquisition presented so far (contact, posture, movement) can be identified automatically via advanced technological solutions such as smart electrodes/sensors and accelerometers. This is not possible for the identification of the ventilation type (tidal breathing, deep breathing or forced maneuver) and, therefore, data-driven approaches are used: the ventilation type is inferred from the analysis of the EIT measurements as described in the following section.

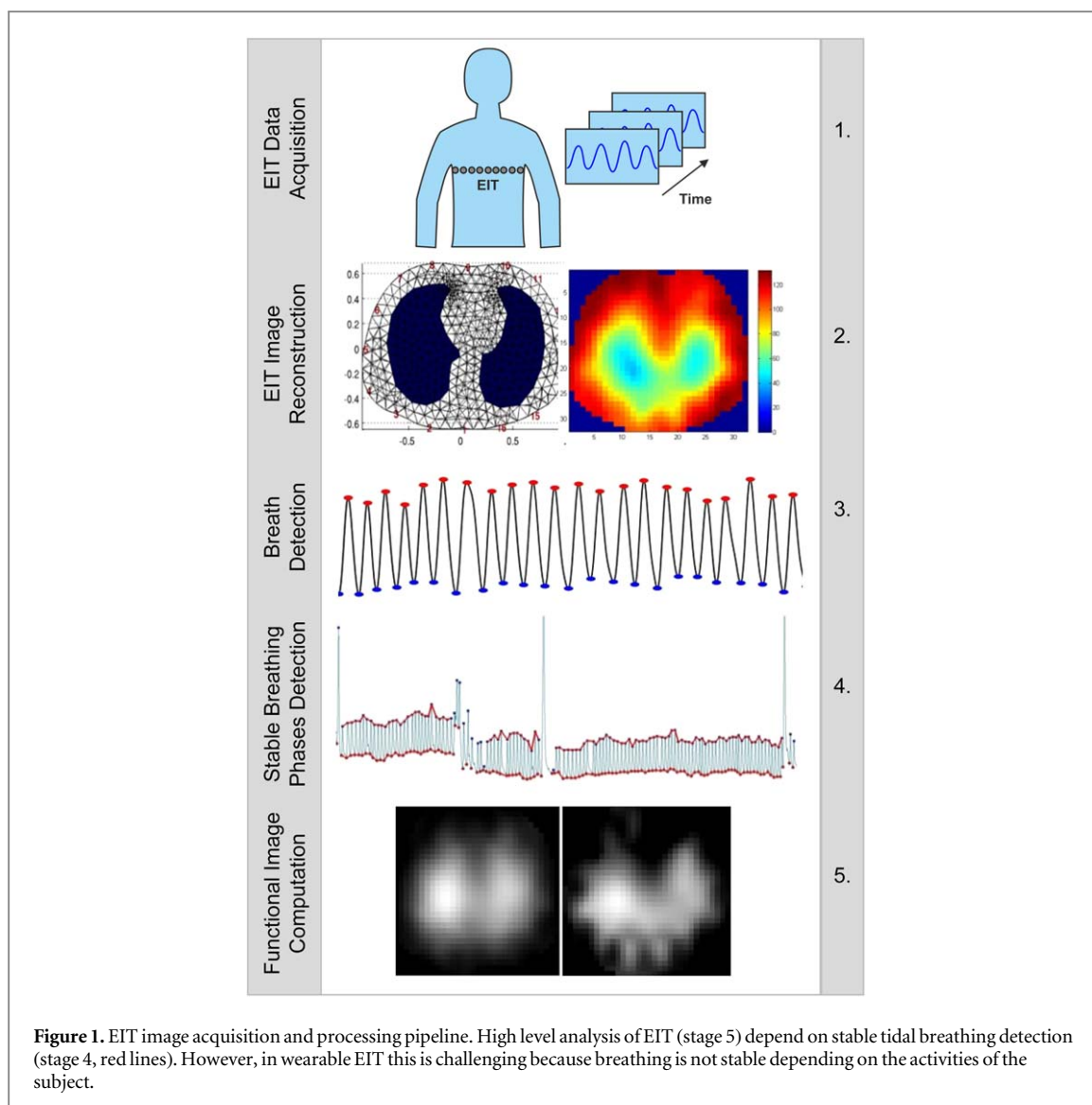
In addition, it is possible that other activities such as speaking, eating or coughing take place in parallel with otherwise stable tidal breathing. In order to detect these activities additional sensors are required which increases complexity as well as intrusiveness, potential points of failure, and patient discomfort, and therefore, it is desirable not only to study whether or not they affect EIT recordings but also to investigate the feasibility of recognizing their presence in the EIT signals. Or at least, whether it is possible to discriminate stable tidal breathing periods (STBPs) from all other breathing patterns. Fast and simple algorithmic solutions are preferable due to the distributed nature of most remotely monitoring projects where a number of wearable vests are continuously recording and transmitting biomedical data (EIT, ECG, PPG, lung sounds, etc).

The aim of this study was twofold: (i) to examine the feasibility of identifying STBPs using features extracted from the EIT global impedance waveform (GIW) or similar EIT summary representations and (ii) to develop a method for the automated identification of such periods with minimal number of parameters. The proposed identification method, the EIT data acquisition protocol, and the techniques for its statistical analysis are presented in detail in section 2. In section 3, the results of the application of the proposed method are presented, and our observations are discussed, analyzed and possible future directions are suggested.

2. Methods

2.1. Subjects

The study was carried out within the framework of the European Union projects WELCOME (Grant No. 611223) and WELMO (Grant No. 825572) aiming to develop an integrated care approach for continuous monitoring, early diagnosis and detection of worsening events and treatment of patients suffering from chronic obstructive pulmonary disease. It was approved by the Institutional Ethics Committee and informed written consent was obtained from each study participant. We analyzed 69 ten-minute recordings of EIT data obtained in 10 lung-healthy adult subjects (4 men, 6 women) with no history of lung disease and average age of 40 ± 9 years, body height of 176 ± 13 cm and body weight of 70 ± 15 kg.

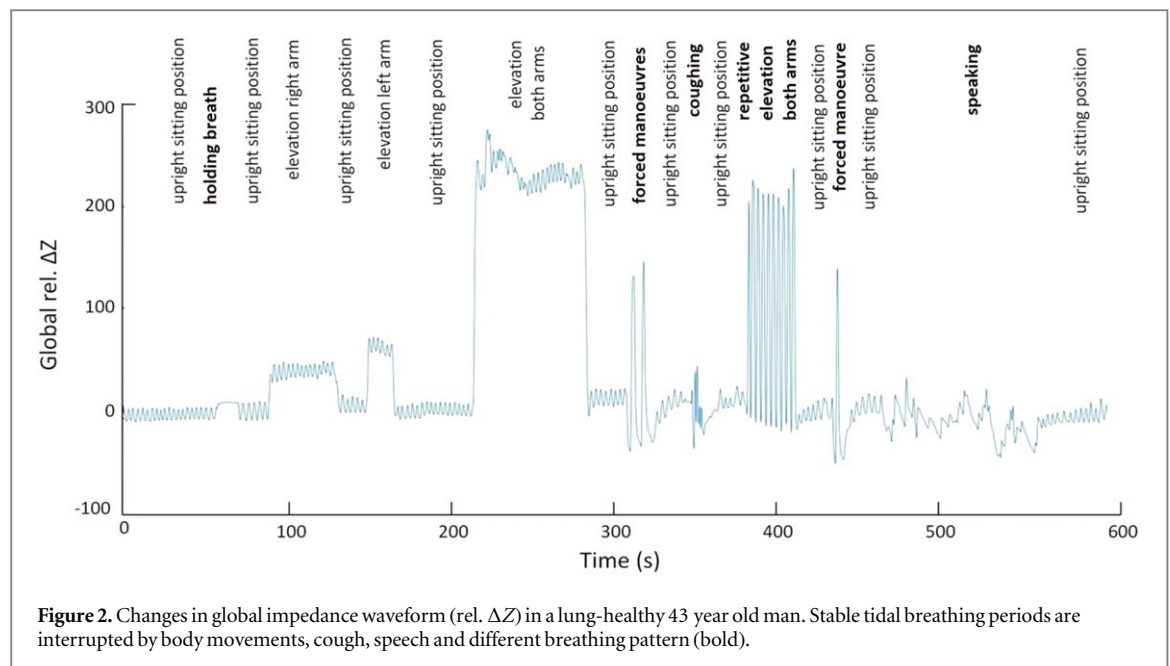


2.2. EIT measurements and reconstruction

The Goe-MF II EIT system (CareFusion, Höchberg, Germany) was used for EIT data acquisition. An array of sixteen self-adhesive electrodes (Blue Sensor L-00-S, Ambu, Ballerup, Denmark) were placed around the chest circumference at the level of the fifth to sixth intercostal space of each studied subject (figure 1, stage 1). The reference electrode was placed on the right side of the abdomen. The reference electrode in the GoeMF II system serves the same role as the driven right leg electrode in most clinical ECG systems; it is used to reduce the common-mode signal level in the body so that any residual non-zero common mode gain the input amplifier has less effect on the signal. Current injections with amplitude $5 \text{ mA}_{\text{rms}}$ at a frequency of 50 kHz were applied through adjacent pairs of electrodes in a sequential rotating process and the resulting potential differences were measured by the remaining electrodes (adjacent current stimulation pattern). The EIT scan rate was 33 images s^{-1} and each of the 69 recording sessions had a duration of 10 min. Raw EIT images/frames were reconstructed using the Graz Consensus Reconstruction Algorithm (GREIT) as implemented in the EIDORS public software (Adler and Lionheart 2005, 2006, Adler *et al* 2009, Gomez-Laberge *et al* 2012). The reconstruction used an adult thorax shaped model with a single plane of 16 electrodes and the adjacent stimulation pattern (figure 1, stage 2, Left). In each 32×32 EIT, the non-zero pixels showed the normalised difference between the instantaneous and baseline pixel impedance (i.e. the relative impedance change). The baseline pixel impedance was equivalent to the average pixel impedance determined during a selected STBP.

2.3. Protocol

The examined subjects were instructed to perform different ventilation and non-ventilation manoeuvres during the data acquisition at random order. As shown in figure 2, a typical sequence included:



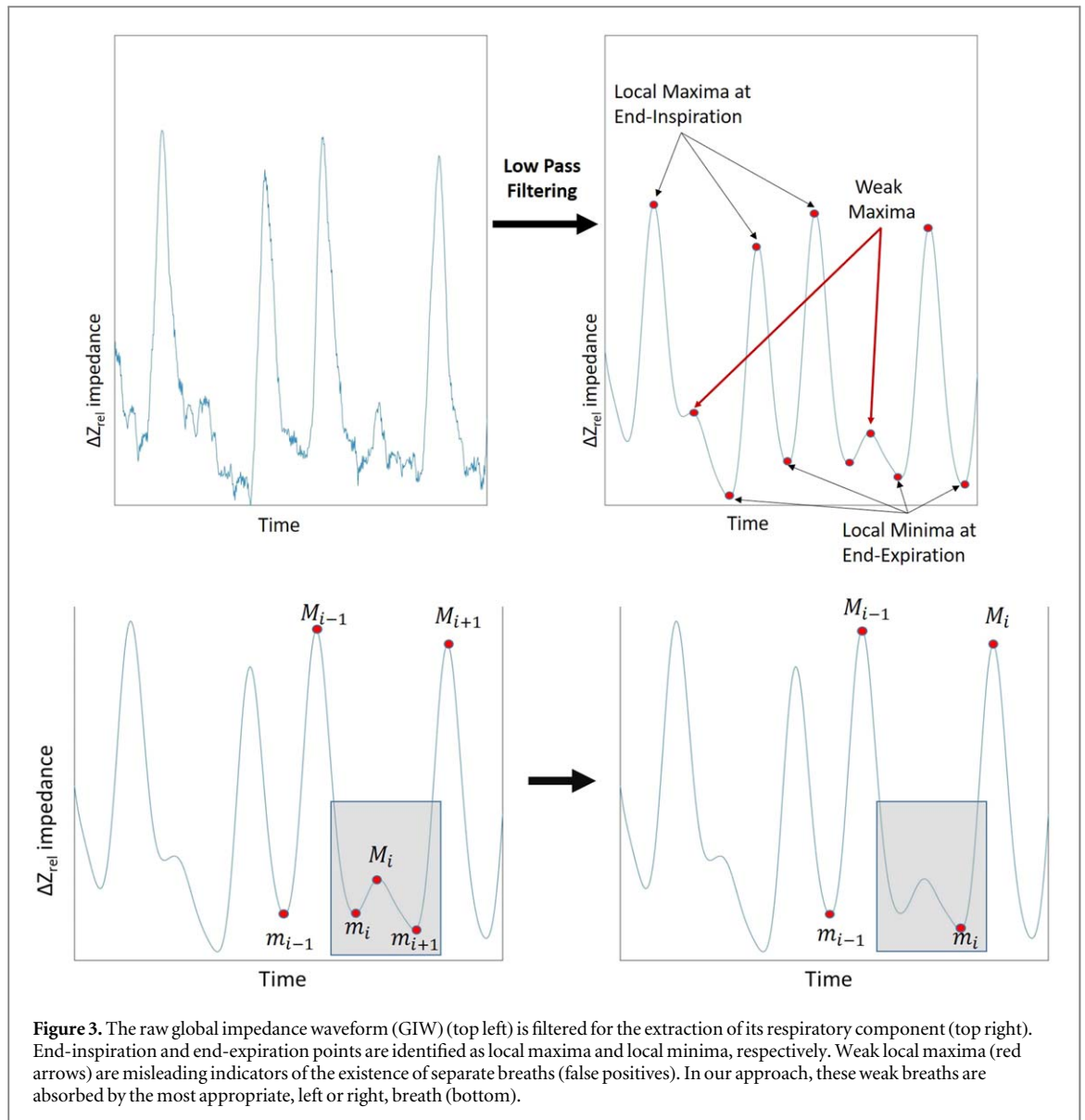
- Stable tidal breathing in upright sitting position,
- breath holding,
- elevation of arms (left, right or both) one or more times continuously,
- forced full inspiration and expiration manoeuvres,
- coughing,
- speaking, laughing, eating
- change in posture (seated to standing and vice versa, torso rotation).

The start and end time points of each of the mentioned manoeuvres together with their description were manually recorded by the expert physician supervising the EIT data acquisition process.

2.4. Data analysis

The standard EIT image acquisition and processing pipeline is shown in figure 1. It is emphasized that in wearable EIT systems, the overall EIT processing pipeline must be *automated*, since there is no possibility of user interaction of any type. The automatically reconstructed EIT image sequence is the output of stage 2 where the reconstruction algorithm is applied to the raw voltage measurements provided at stage 1. At stage 3, the GIW is computed and processed by low-pass filtering for the isolation of its respiratory component. The cutoff frequency was determined automatically based on the magnitude of the Fourier-transformed raw GIW to identify the frequency with the largest spectral peak f_{\max} and set to $2f_{\max}$ (Gomez-Laberge *et al* 2012)⁶. It is reminded that the GIW represents the relative impedance ΔZ_{rel} as a function of time, since for each 32×32 EIT image frame the average value is stored (Frerichs *et al* 2017, Khodadad *et al* 2018). Breath detection is achieved by computing the local minima and local maxima of the respiratory GIW, since they correspond to end-expiratory and end-inspiratory points, respectively (Hahn *et al* 1996). After the elimination of false positive (or weak) breaths (see subsequent subsection), the remaining breaths constitute the output of stage 3. At stage 4, the respiratory GIW together with the detected breaths sequence is processed for the extraction and identification of STBPs. As mentioned before, stage 4 is the main focus of the current study (feasibility of automatic detection in wearable EIT and accuracy). In the following subsections, the terminology and computational steps of stages 3 and 4 are presented in detail.

⁶ The MATAB source code for filtering can be found at the EIDORS website (http://eidors3d.sourceforge.net/tutorial/lung_EIT/cg_2012_ards_recruitment.shtml).



2.4.1. Breath detection and weak breath elimination

As mentioned in the previous paragraph, a frequent complication in breath detection from the respiratory GIW is the existence of weak local maxima that survived the low-pass filtering depending on the relative positions of respiratory and cardiac rate harmonics. An indicative example is shown in figure 3. The respiratory component (figure 3, top right) of the raw GIW (figure 3, top left) is the result of the application of low-pass filtering to eliminate the higher frequency cardiac component of the raw GIW. The indicated local maxima (red arrows) cannot be accepted as end-inspiration points of regular breaths since they are too weak (low amplitude) and too short (brief duration) based on precalculated thresholds for amplitude and duration, respectively. In other words, they are false positives and, therefore, they are eliminated in the sense that they are considered part of the appropriate neighboring (left or right) breath. This retrospective merging process is illustrated in figure 3 (bottom). The false positive weak breath i defined by local minimum m_i and local maximum M_i is considered part of breath $i - 1$ resulting in relabeling the initially detected breath $i + 1$ as breath i .

A candidate breath i with start-inspiration at time m_i , end-inspiration at M_i and end-expiration at m_{i+1} is considered *weak* if the tidal gas volume exhaled or inhaled is less than a threshold V_{weak} (figure 4). Mathematically, the minimum tidal volume V_i^{min} defined as $V_i^{min} = \min(V_i^{insp}, V_i^{exp})$, where V_i^{insp} , V_i^{exp} are the gas volumes corresponding to the inspiration and expiration phases of breath i must be less than V_{weak} . By denoting the respiratory component of GIW as G , we obtain (figure 4):

$$V_i^{insp} = G(M_i) - G(m_i), \quad V_i^{exp} = G(M_i) - G(m_{i+1}).$$

For the determination of threshold V_{weak} , we assume that more than 50% of the total number of detected candidate breaths belong in stable breathing periods. In this way, the median value of the tidal gas volume

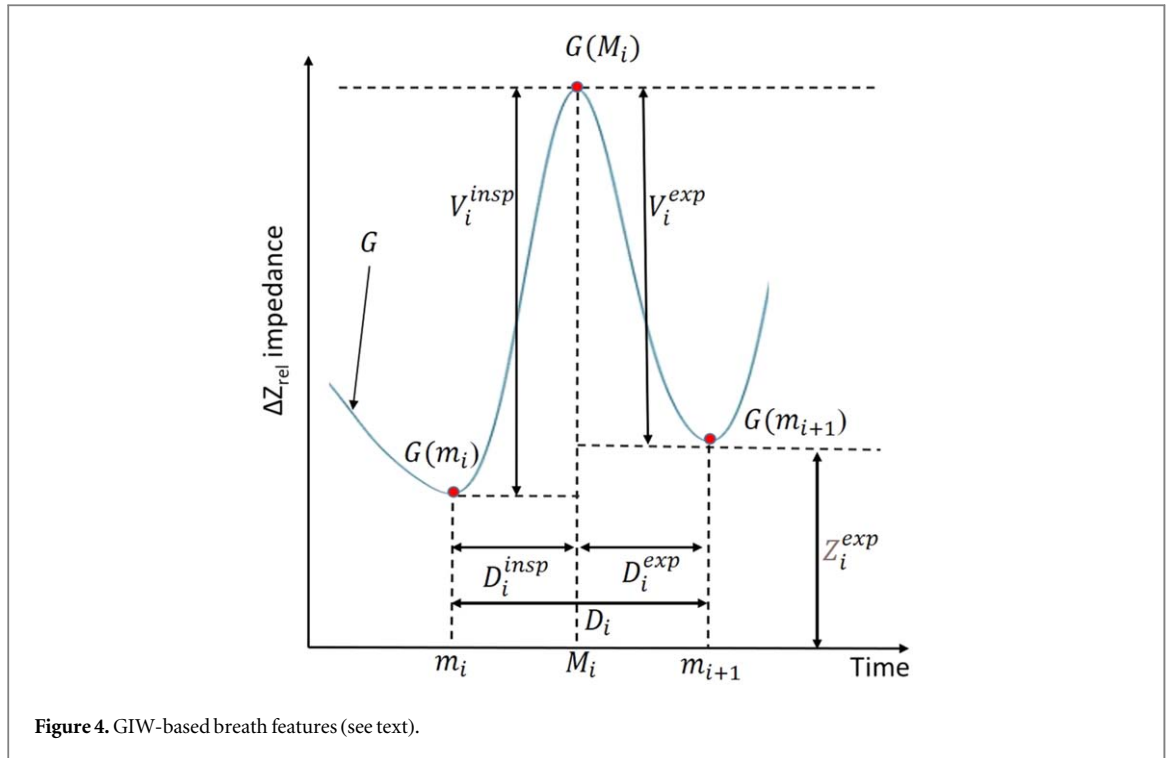


Figure 4. GIW-based breath features (see text).

exhaled or inhaled for the whole set of candidate breaths is an accurate estimate of this gas volume for tidal breaths. It is noted that the retrospective processing of the initially detected breaths allows the computation of the threshold V_{weak} , thus eliminating the weak breaths via a second pass of the breath sequence. Also, in this way, other types of breaths (such as forced manouevres) may be subsequently detected and processed. This is not possible with ‘real time’ breath detection and elimination where breaths are detected based on maxima and minima of the last seconds of the GIW (Dräger 2021).

2.4.2. GIW-based breath features

The identification of the STBPs was based on breath feature variation analysis using a moving (sliding) window approach. Specifically, the GIW-derived features for breath b_i were:

- the tidal volume, V_i , defined as the *maximum* of tidal gas volume exhaled or inhaled, that is, $V_i = \max(V_i^{insp}, V_i^{exp})$,
- the breath duration, $D_i = m_{i+1} - m_i$ which is the sum of the durations of the inspiration and expiration phases D_i^{insp} , D_i^{exp} , respectively (figure 4), and
- the end-expiratory impedance level, $Z_i^{exp} = G(m_{i+1})$.

The desired ventilation homogeneity of a breathing period (i.e. of a sequence of consecutive breaths) can be characterized by the coefficient of variation (CV) of tidal volume, CV_V , duration, CV_D and end-expiratory impedance level, CV_Z . It is reminded that the CV of a distribution is defined as the ratio of the standard deviation of the distribution over its mean. For the sequence of consecutive breaths of a STBP, $B = (b_1, b_2, \dots, b_n)$, the above CVs are expressed as

$$CV_V = \frac{SD(V_1, V_2, \dots, V_n)}{Mean(V_1, V_2, \dots, V_n)},$$

$$CV_D = \frac{SD(D_1, D_2, \dots, D_n)}{Mean(D_1, D_2, \dots, D_n)},$$

$$CV_Z = \frac{SD(Z_1, Z_2, \dots, Z_n)}{Mean(Z_1, Z_2, \dots, Z_n)},$$

where V_i , D_i , Z_i are the tidal volume, duration and end-expiration impedance of breath b_i for $i \in \{1, 2, \dots, n\}$. $Mean(\cdot)$, $SD(\cdot)$ represent the sample mean and sample standard deviation of their arguments.

2.4.3. Stable breathing period detection

The sequence of detected breaths, $S = (b_1, b_2, \dots, b_N)$, is input to a sliding window algorithm where S is scanned from left to right: at each position i , $i = 1, \dots, N - W + 1$, the sequence of consecutive breaths

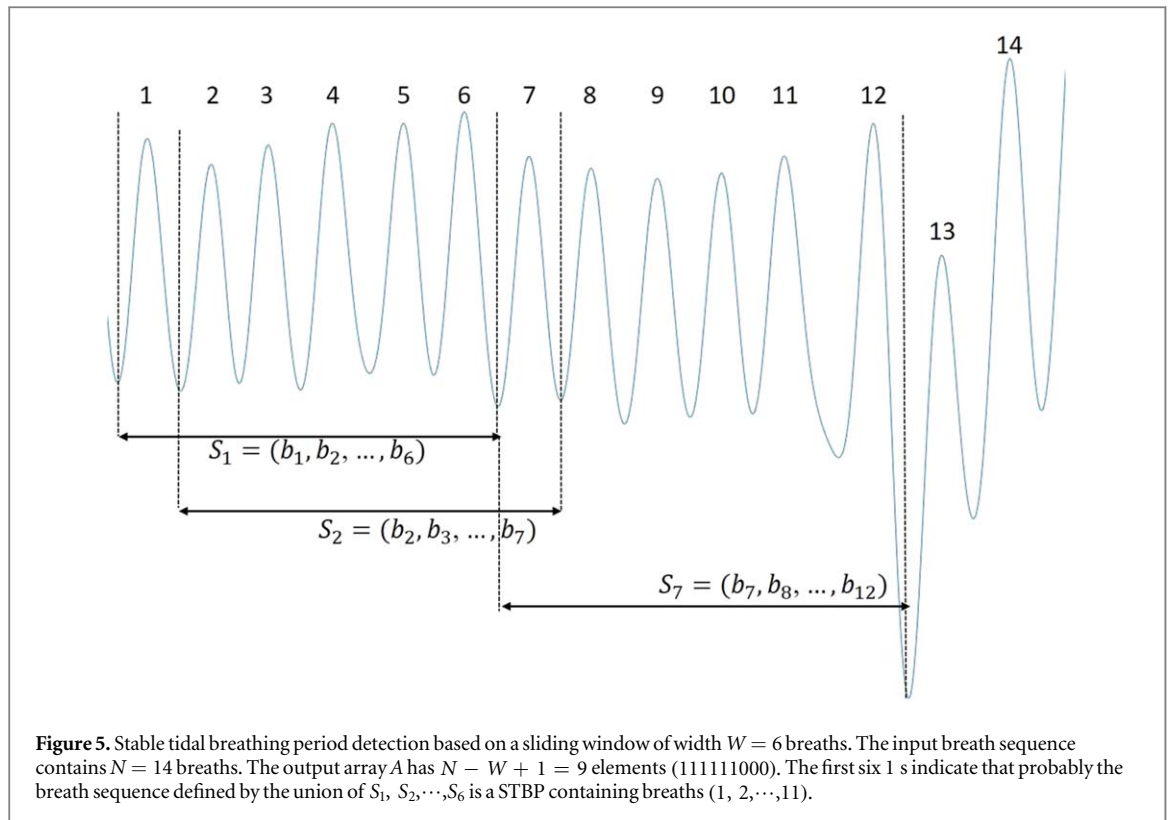


Figure 5. Stable tidal breathing period detection based on a sliding window of width $W = 6$ breaths. The input breath sequence contains $N = 14$ breaths. The output array A has $N - W + 1 = 9$ elements (11111000). The first six 1s indicate that probably the breath sequence defined by the union of S_1, S_2, \dots, S_6 is a STBP containing breaths (1, 2, ..., 11).

$S_i = (b_i, b_{i+1}, \dots, b_{i+W-1})$ constitutes the current window of width W for which it is decided if it is a STBP of length W or not, according to the following rule:

$$S_i \text{ is STBP IF } (CV_V < T_V) \text{ and } (CV_D < T_D) \text{ and } (CV_Z < T_Z), \quad (1)$$

where T_V, T_D, T_Z are predetermined thresholds for the CV of tidal volume, duration and end-expiration rel. impedance, respectively.

The output of the above scanning algorithm is an array A of size $N - W + 1$ with the following values

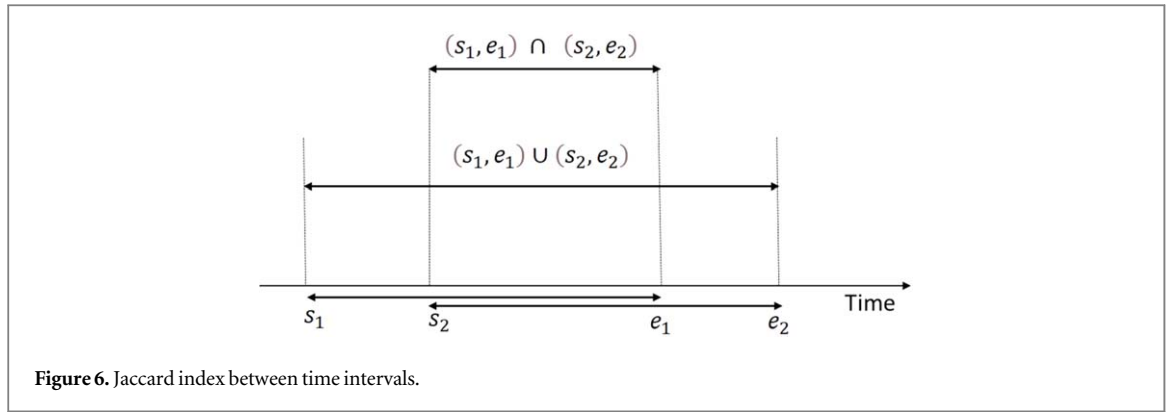
$$A[i] = \begin{cases} 1, & \text{if } S_i \text{ is STBP} \\ 0, & \text{otherwise} \end{cases}$$

In other words, $A[i]$ is 1 if the sequence of consecutive breaths that correspond to S_i which is $(b_i, b_{i+1}, \dots, b_{i+W-1})$ is STBP. It is expected that sequences of consecutive 1s in A signify the existence of longer stable breathing periods since neighboring 1s indicate highly overlapping STBPs. Specifically, if both $A[i]$ and $A[i + 1]$ equal to 1, then we expect $S_i \cup S_{i+1} = (b_i, b_{i+1}, \dots, b_{i+W})$ be STBP of length $W + 1$. By generalizing this heuristic merging rule, for a sequence of m consecutive 1s in A , we expect the breath sequence $S_i \cup S_{i+1} \cup \dots \cup S_{i+m} = (b_i, b_{i+1}, \dots, b_{i+W-1+m})$, be STBP of length $W + m - 1$. For this reason, in the last step of the STBP detection algorithm STBPs defined by consecutive 1s in A are identified and merged to longer STBPs (figure 5).

2.4.4. Evaluation

The final output of the proposed STBP detection method (i.e. the output of stage 4 in figure 1) is a set of detected STBPs where each STBP is defined by a sequence of consecutive breaths as presented in detail in the previous section. To assess the performance of the method, we applied the method to 69 EIT recordings of duration 10 min each. In these recordings, the true STBPs were not identified as sequences of consecutive breaths. Instead, the expert manually described them as *time intervals* by their start and end time points (in seconds). For this reason, the algorithmically detected STBPs were also represented as time intervals. Given two STBPs, P_1, P_2 , represented as time intervals, $P_1 = (s_1, e_1), P_2 = (s_2, e_2)$ where s_1, s_2 are their starting and e_1, e_2 their end time points, respectively, their *Jaccard similarity index* is defined by

$$\begin{aligned} J(P_1, P_2) &= J((s_1, e_1), (s_2, e_2)) \\ &= \frac{|(s_1, e_1) \cap (s_2, e_2)|}{|(s_1, e_1) \cup (s_2, e_2)|} \end{aligned}$$



where $|(s_1, e_1) \cap (s_2, e_2)|$ represents the duration of the overlap in time between the two intervals (figure 6) and $|(s_1, e_1) \cup (s_2, e_2)|$ their total duration. Jaccard index can be values between 0 (no overlap) and 1 (time intervals coincide). In our case, the following *modified Jaccard similarity index* was used

$$J_m(P_{\text{True}}, P_{\text{Detected}}) = J((s_T, e_T), (s_D, e_D)) \\ = \frac{|(s_T, e_T) \cap (s_D, e_D)|}{|(s_T, e_T)|}$$

where $P_{\text{True}} = (s_T, e_T)$, $P_{\text{Detected}} = (s_D, e_D)$ are time intervals corresponding to a true and a detected STBP, respectively. Positive values of J_m indicate that part of the corresponding true STBP has been detected. The maximum value of J_m is 1 indicating complete detection of the corresponding true STBP (figure 9, STBPs 1, 2, 8 and 9). On the other hand, zero values of J_m identify false positives i.e. identified STBPs that are not true (figure 9, STBPs 3 and 4).

2.4.5. Global inhomogeneity (GI) and fraction of ventilation indices

The calculation of the widely used ventilation heterogeneity measure, namely, the GI index, for each breath is based on the corresponding tidal image, DI , a functional image each pixel of which represents the difference in impedance between end-inspiration and end-expiration (Zhao et al 2009). Initially, the median value, $med(DI_L)$, of pixels belonging to the lung area L of this image is computed. Then, the normalized sum of the absolute difference between the computed median value and every pixel value, DI_{xy} , is considered to indicate the variation in the tidal volume distribution in the whole lung region:

$$GI = \frac{\sum_{x,y \in L} |DI_{xy} - med(DI_L)|}{\sum_{x,y \in L} DI_{xy}}$$

where the required lung area, L , is identified according to Zhao et al (2010).

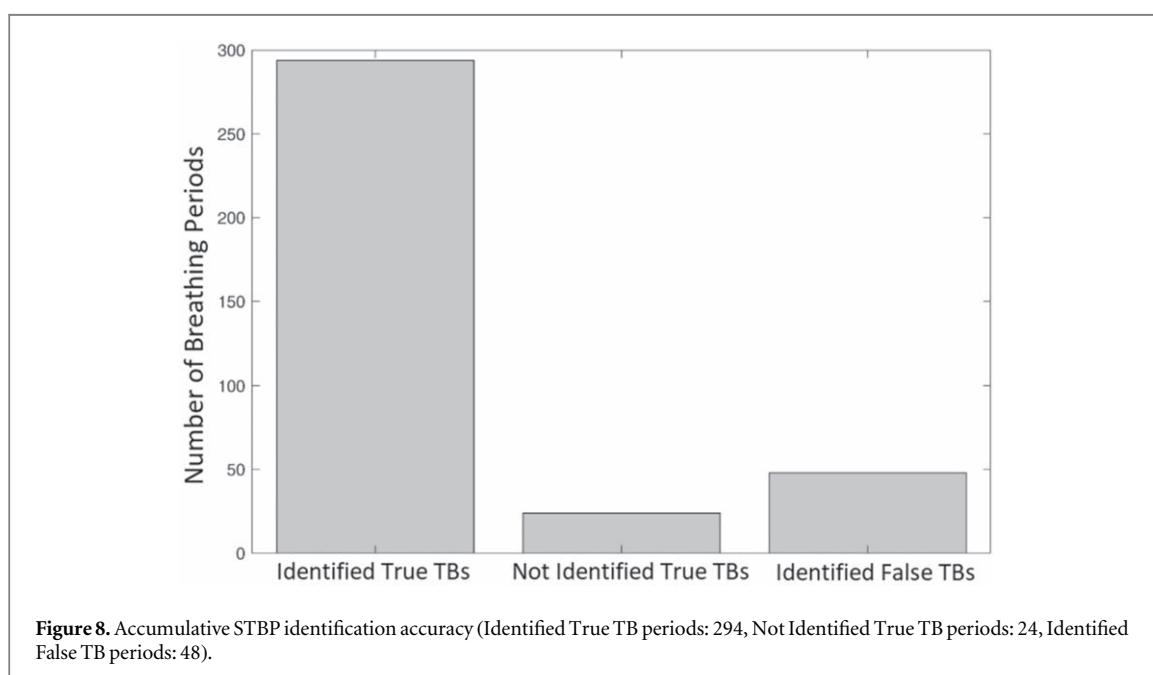
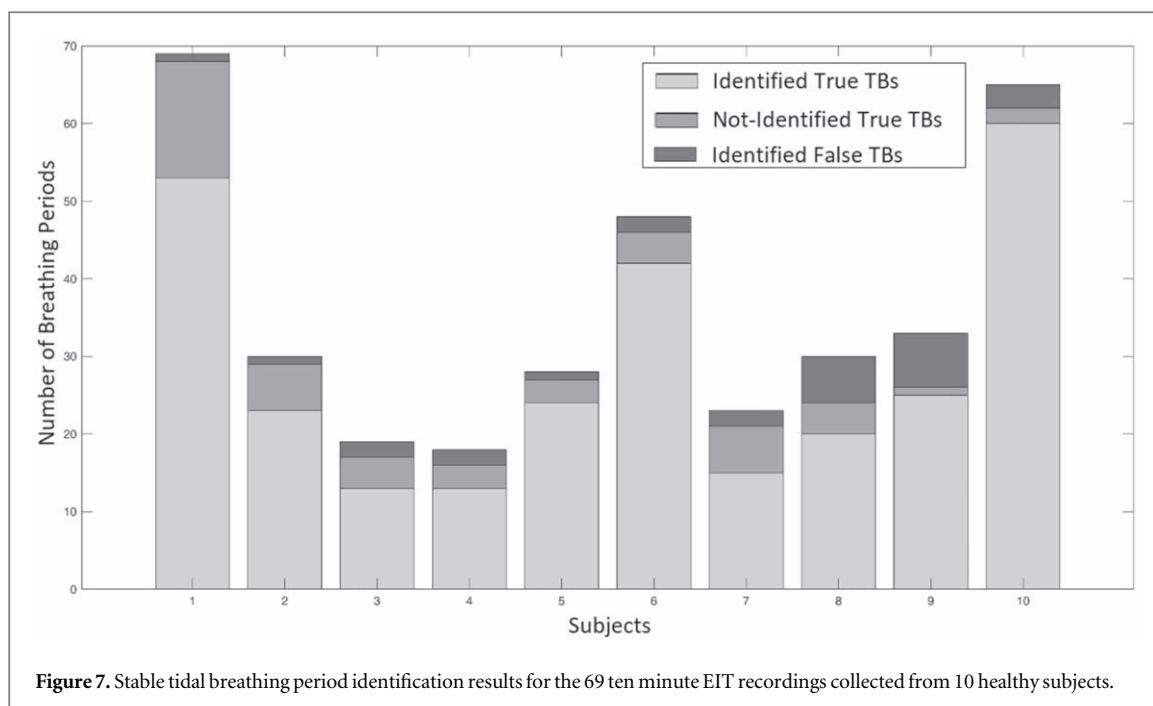
The right ventilation fraction represents the fraction of ventilation volume that corresponds to the right side of the chest and is computed by the ratio of the sum of the values of the right half of the tidal image DI over the total sum.

2.4.6. Statistical analysis

The proposed STBP identification method was implemented in MATLAB R2019a (MathWorks, Natick, MA). EIT reconstruction was based on GREIT as implemented in EIDORS. Data was tested for normality using the D'Agostino & Pearson normality test and between-group comparisons were performed using one-way ANOVA. Data was analysed using MATLAB R2019a and GraphPad Prism 9.

3. Results and discussion

The proposed stable tidal breathing method was applied to 69 ten minute EIT recordings collected from 10 healthy volunteers. The total number of true stable breathing periods identified by the expert was 318. Figure 7 shows the STBP identification results as distributed in the 10 healthy subjects. All programs executed offline on a personal computer with average processing time less than one second per each 10 min EIT recording. In total, 294 STBPs were correctly identified (true positives) giving a success rate equal to 92.45% approximately (figure 8). All correctly identified STBPs had positive modified Jaccard similarity index with 84% of them having value greater than 0.8. The number of false positives (not stable breathing periods that were identified as stable) was 48. The thresholds T_V , T_D , T_Z of the CVs in equation (1) were set to 0.25, 0.25, 0.2 and the size of the sliding



window W was set to 6. This means that all detected STBPs consist of W consecutive breaths or more and therefore, true STBPs containing less than 6 breaths (i.e. with duration less than 20–30 s) are not detected. Experiments with smaller values of the sliding window W (4 and 5), exhibited slightly better accuracy (around 94%), however, this was achieved at the cost of a large increase of false positives, mostly during speaking and eating. This was expected, since depending on the particular way of speaking or eating of each subject, breathing periods of 3, 4 or 5 breaths may be projected in the GIW as STBPs. On the other hand, values of W greater than 8 excluded STBPs of length 6, 7 and 8 which were frequent among the true STBPs. Concerning the other parameters, namely, T_V , T_D , T_Z , we experimentally observed weak sensitivity of the accuracy on the threshold values in the range [0.2, 0.3] indicating that STBPs and non-STBPs are sufficiently separated with respect to volume, duration and end-expiratory impedance level. The values used for the results reported above were specified using the empirical risk minimization based on the annotated data.

Figure 9 shows an indicative STBP identification result for one of the 69 EIT recording sessions of 10 min duration. The true STBPs identified by the expert are indicated by enclosing rectangles while the detected STBPs are indicated by a pair of red lines connecting the end-expiration and end-inspiration points of their respiratory

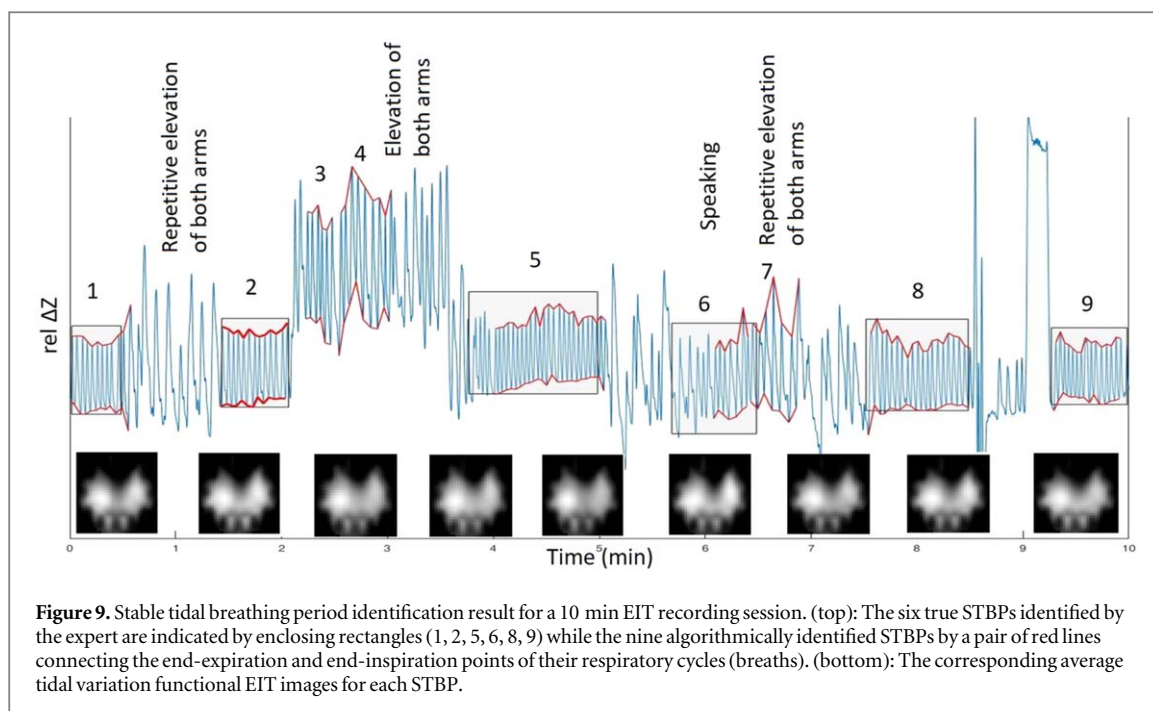


Figure 9. Stable tidal breathing period identification result for a 10 min EIT recording session. (top): The six true STBPs identified by the expert are indicated by enclosing rectangles (1, 2, 5, 6, 8, 9) while the nine algorithmically identified STBPs by a pair of red lines connecting the end-expiratory and end-inspiration points of their respiratory cycles (breaths). (bottom): The corresponding average tidal variation functional EIT images for each STBP.

cycles (breaths). In some cases, the expert considered that stable breathing can coexist with speaking depending on the shape and form of the GIW displayed in real time by the acquisition device during recording. The corresponding average TV functional EIT images for each STBP are almost identical (figure 9, bottom) implying that such phases are also suitable for reliable assessment of ventilation distribution during tidal breathing.

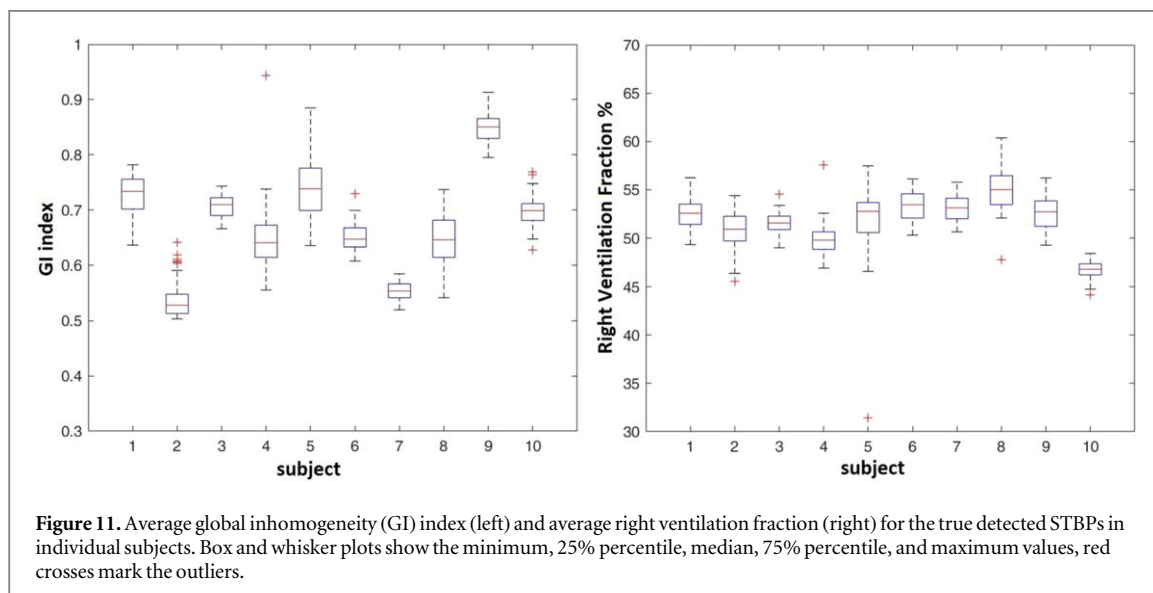
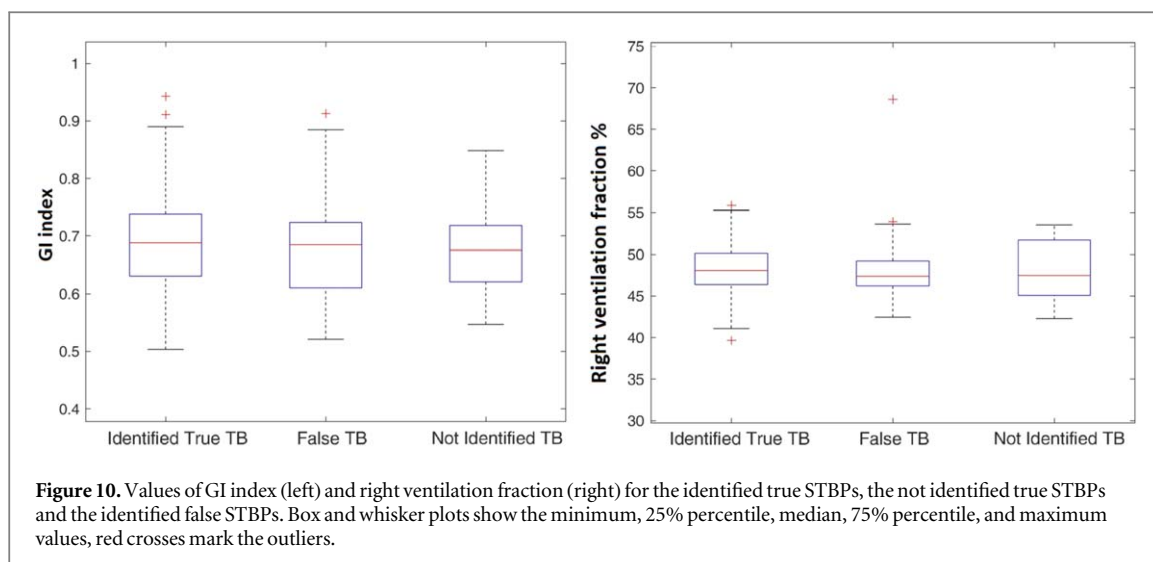
Another feature of interest in automated EIT data analysis is the accuracy in identifying the most stable STBP, in the sense of minimum tidal volume variation. This is useful in cases where a STBP must be automatically selected and analyzed (figure 9, STBP 2, thicker red lines). In the results reported above, 66 out of 69 identified most stable STBPs were true STBP (95.66 % accuracy).

In addition to eating and speaking, another source of false positives in STBP identification is the ‘elevation of both arms’ posture. According to our observations, the corresponding breathing pattern may fulfill the requirements of a STBP as defined by equation (1) (figure 9, STBP 3). However, in many cases, the average end-expiratory impedance of STBPs at ‘elevation of both arms’ posture is considerably higher, making their detection possible.

For the detection and elimination of weak breaths (section 2.3), the proposed method depends on the threshold V_{weak} which is used to decide if a candidate breath i having minimum tidal volume V_i^{min} is weak or not. This parameter was determined by calculating the median value of the minimum tidal volume V^{min} of the whole set of detected breaths in the 10 min recording session under analysis. It is well-known that the median is a robust estimator of the average value in the presence of outliers under the condition that these outliers represent a portion that is less than 50% of the sample size. In our case, outliers are produced by breaths belonging to breathing patterns other than stable STBPs: all patterns described in section 2.2. Under this condition, we found that a value of V_{weak} equal to the one third of the computed median discriminates effectively weak breaths. In ‘real time’ breath detection, less accurate weak breath detection is expected, unless the breathing pattern is highly regular and stable. This is the case in ICUs where mechanical ventilation is used and there are no other activities (speaking, arm /body movement, etc). However, when the majority of breaths in the recording session correspond to non-STBPs such as speaking, eating, moving (arms or torso), coughing and forced ventilation manoeuvres, the estimation of value V_{weak} may become highly erroneous.

Figure 10 shows two EIT measures of ventilation distribution, the average GI index (left) and average right ventilation fraction (right) for the identified true STBPs, the not identified true STBPs and the identified false STBPs. Statistical analysis revealed no significant differences among the groups both for GI (ANOVA, p -value = 0.640) and the Right ventilation fraction (ANOVA, p -value = 0.258). Since the examinations were carried out in healthy subjects with no history of lung diseases and without any study-related interventions known to induce redistribution of ventilation in the chest cross-section, such as horizontal postures, this finding was anticipated and confirms the plausibility of EIT-based assessment of ventilation homogeneity (Zhao *et al* 2009, Reifferscheid *et al* 2011, Lupton-Smith *et al* 2014).

Figure 11 shows the average GI and right ventilation fraction per subject. It is evident that there are statistically significant differences between different subjects. This means that the value of these two indices may



be subject dependent and therefore, any method for establishing population wide ‘normal’ values should take this inter-subject distribution variability feature into account. The possible causes for the observed interindividual differences are related to age, chest anatomy and the exact location of the EIT examination plane. It has been shown in previous studies that even small changes in the placement of EIT electrodes in the craniocaudal direction exert an effect on the observed ventilation distribution pattern (Reifferscheid *et al* 2011, Krueger-Ziolek *et al* 2015, Karsten *et al* 2016). In view of the recent development of EIT systems, where the electrodes are integrated into wearable garments, the possible effect of placing the electrodes at slightly different chest locations during repeated examinations can be expected to be minimized because of the fixed electrode positions in the wearable (Rapin *et al* 2019, Frerichs *et al* 2020).

In order to be able to obtain reliable diagnostic and monitoring information on the lung function status from EIT examinations conducted in spontaneously breathing subjects in the future expected remote setting, reference EIT values are urgently needed. The first attempts of creating such values have been accomplished (Yang *et al* 2021), however, much larger cohorts of healthy women and men of different ages and body sizes will have to be examined. The generation of such reference values will require examinations in multiple body positions because postural changes induce shifts in intrathoracic and abdominal organs whereby not strictly identical lung tissue regions are assessed by EIT. Consequently, EIT parameters are expected to vary among postures. Ideally, the body posture should be captured along with the EIT data which would ease the interpretation of the findings.

This study has a few limitations. First of all, the limited amount of data since: (i) it was based on healthy volunteers, (ii) the breathing pattern and sequence of movements (arms and torso) was designed to serve as first

of its kind feasibility study and (iii) the recorded EIT measurements were performed in an upright position only. Many other horizontal postures (supine, prone, right and left lateral) are possible and are expected to affect the findings due to gravity-dependent redistribution of ventilation (Frerichs *et al* 1996, Reifferscheid *et al* 2011, Lupton-Smith *et al* 2014). Another limitation concerns the timing procedure used by the expert during data acquisition. As expected, the manual time recording process was not error free. The introduced inaccuracies were most of the time less than 3–4 s. The error assessment was based on the manual comparison of the time of occurrence of characteristic short manoeuvres such as Forced Manoeuvres as recorded from the EIT device. In our study, we used the relatively old Goe-MF II device which certainly is outperformed by currently available modern EIT devices. However, this imitation did not pose any disadvantage in view of the major goal of the study which was to develop procedures capable of identifying stable breathing periods suitable for analysis of regional ventilation. Such procedures are universal and device-independent and could be applied to EIT measurements accomplished with any EIT device.

Despite its limitations, the present study showed that the accurate automated stable STBP identification is feasible. Also, it revealed that the breathing patterns (as projected to the GIW) caused by specific manoeuvres such as speaking, eating and ‘both arm elevation’ may appear as stable. This constitutes valuable information for extracting recommendation guidelines and designing the most appropriate sequence of ventilation manoeuvres during wearable EIT recording sessions in which the presence of false STBP sources is minimised. In addition, the observed inter-subject ventilation distribution variability in combination with the fact that the ultimate goal of monitoring is early identification of lung disease deterioration, indicates that machine learning techniques based on personalized training datasets may be a promising future research direction.

4. Conclusion

Our study findings imply that automated selection of undisturbed, STBPs, by processing the EIT GIW is feasible when spontaneously breathing subjects are monitored by EIT. Such stable phases of EIT data can be used to generate various measures characterizing regional lung function over time such as GI index, fraction of ventilation, center of ventilation and functional EIT images. Time-dependent changes in these measures might be applied to identify lung disease deterioration or to assess the therapy effects. Preliminary results indicate that a personalized approach should be adopted since the numerical measures seem to be subject/patient dependent. In addition, specific activities such as speaking and eating can also be sources of stable breathing patterns, an information that should be taken into account.

Acknowledgments

We thank all the examined healthy subjects for participating in the study. This study was supported by the European Union’s Horizon 2020 Research and Innovation Programme (Project WELMO, Grant Agreement No. 825572).

ORCID iDs

K Haris  <https://orcid.org/0000-0002-9806-6272>

D Pessoa  <https://orcid.org/0000-0002-7783-7488>

B Rocha  <https://orcid.org/0000-0003-1643-667X>

G Petmezas  <https://orcid.org/0000-0002-3371-569X>

I Frerichs  <https://orcid.org/0000-0002-7712-6539>

References

- Adler A 2004 Accounting for erroneous electrode data in electrical impedance tomography *Physiol. Meas.* **25** 227–38
- Adler A *et al* 2009 GREIT: a unified approach to 2D linear EIT reconstruction of lung images *Physiol. Meas.* **30** S35–55
- Adler A and Lionheart W R B 2005 EIDORS: towards a community-based extensible software base for EIT *6th Conf. on Biomedical Applications of Electrical Impedance Tomography (London, UK)*
- Adler A and Lionheart W R B 2006 Uses and abuses of EIDORS: an extensible software base for EIT *Physiol. Meas.* **27** S25–42
- Becher T *et al* 2015 Influence of tidal volume on ventilation inhomogeneity assessed by electrical impedance tomography during controlled mechanical ventilation *Physiol. Meas.* **36** 1137–46
- Blankman P *et al* 2013 Ventilation distribution measured with EIT at varying levels of pressure support and neurally adjusted ventilatory assist in patients with ALI *Intensive Care Med.* **39** 1057–62
- Brown B H 2003 Electrical impedance tomography (EIT): a review *J. Med. Eng. Technol.* **27** 97–108

- Chouvarda I et al 2015 Combining pervasive technologies and cloud computing for COPD and comorbidities management *Proc. 2014 4th Int. Conf. on Wireless Mobile Communication and Healthcare—'Transforming Healthcare Through Innovations in Mobile and Wireless Technologies' MOBIHEALTH 2014* pp 352–6
- Dräger 2020 *Instructions for Use PulmoVista 500 Electrical Impedance Tomograph Software 1.3n* 1st edn (Lübeck: Dräger) pp 1–173
- Frerichs I et al 2016 Regional lung function determined by electrical impedance tomography during bronchodilator reversibility testing in patients with asthma *Physiol. Meas.* **37** 698–712
- Frerichs I et al 2017 Chest electrical impedance tomography examination, data analysis, terminology, clinical use and recommendations: consensus statement of the translational EIT development study group *Thorax* **72** 83–93
- Frerichs I et al 2020 Multimodal remote chest monitoring system with wearable sensors: a validation study in healthy subjects *Physiol. Meas.* **41** 015006
- Frerichs I, Hahn G and Hellige G 1996 Gravity-dependent phenomena in lung ventilation determined by functional EIT *Physiol. Meas.* **17** A149–57
- Gomez-Laberge C, Arnold J H and Wolf G K 2012 A unified approach for EIT imaging of regional overdistension and atelectasis in acute lung injury *IEEE Trans. Med. Imaging* **31** 834–42
- Hahn G et al 1996 Local mechanics of the lung tissue determined by functional EIT *Physiol. Meas.* **17** A159–66
- Hartinger A E et al 2009 Real-time management of faulty electrodes in electrical impedance tomography *IEEE Trans. Biomed. Eng.* **56** 369–77
- Karsten J et al 2016 Influence of different electrode belt positions on electrical impedance tomography imaging of regional ventilation: a prospective observational study *Crit. Care* **20** 3
- Khodadad D et al 2018 Optimized breath detection algorithm in electrical impedance tomography *Physiol. Meas.* **39** 094001
- Kobylianskii J et al 2016 Electrical impedance tomography in adult patients undergoing mechanical ventilation: a systematic review *J. Crit. Care* **35** 33–50
- Krueger-Ziolek S et al 2015 Positioning of electrode plane systematically influences EIT imaging *Physiol. Meas.* **36** 1109–18
- Lasarow L et al 2021 Regional lung function measures determined by electrical impedance tomography during repetitive ventilation manoeuvres in patients with COPD *Physiol. Meas.* **42** 015008
- Lehmann S et al 2016 Global and regional lung function in cystic fibrosis measured by electrical impedance tomography *Pediatric Pulmonol.* **51** 1191–9
- Lupton-Smith A R et al 2014 Challenging a paradigm: positional changes in ventilation distribution are highly variable in healthy infants and children *Pediatric Pulmonol.* **49** 764–71
- Martins T de C et al 2019 A review of electrical impedance tomography in lung applications: theory and algorithms for absolute images *Annu. Rev. Control* **48** 442–71
- Mauri T et al 2013 Topographic distribution of tidal ventilation in acute respiratory distress syndrome: effects of positive end-expiratory pressure and pressure support *Crit. Care Med.* **41** 1664–73
- Pulletz S et al 2010 Effects of restricted thoracic movement on the regional distribution of ventilation *Acta Anaesthesiol. Scand.* **54** 751–60
- Rapin M et al 2019 Wearable sensors for frequency-multiplexed eit and multilead ECG data acquisition *IEEE Trans. Biomed. Eng.* **66** 810–20
- Reifferscheid F et al 2011 Regional ventilation distribution determined by electrical impedance tomography: reproducibility and effects of posture and chest planeresp *Respirology* **16** 523–31
- Vogt B et al 2016 Influence of torso and arm positions on chest examinations by electrical impedance tomography *Physiol. Meas.* **37** 904–21
- Yang L et al 2021 Regional ventilation distribution in healthy lungs: can reference values be established for electrical impedance tomography parameters? *Ann. Transl. Med.* **9** 789
- Yoshida T et al 2013 Spontaneous effort causes occult pendelluft during mechanical ventilation *Am. J. Respiratory Crit. Care Med.* **188** 1420–7
- Zhao Z et al 2009 Evaluation of an electrical impedance tomography-based global inhomogeneity index for pulmonary ventilation distribution *Intensive Care Med.* **35** 1900–6
- Zhao Z et al 2010 A lung area estimation method for analysis of ventilation inhomogeneity based on electrical impedance tomography *J. X-Ray Sci. Technol.* **18** 171–82
- Zhao Z et al 2013 Regional airway obstruction in cystic fibrosis determined by electrical impedance tomography in comparison with high resolution CT *Physiol. Meas.* **34** N107